

# A Hamiltonian description of finite-time singularity in Euler's fluid equations

Philip J. Morrison\*

*Department of Physics and Institute for Fusion Studies,  
The University of Texas at Austin, Austin, TX, 78712, USA*

Yoshifumi Kimura

*Graduate School of Mathematics, Nagoya University,  
Furo-cho, Chikusa-ku, Nagoya 464-8602, Japan*

(Dated: July 18, 2023)

## Abstract

The recently proposed low degree-of-freedom model of Moffat and Kimura [1, 2] for describing the approach to finite-time singularity of the incompressible Euler fluid equations is investigated. The model assumes an initial finite-energy configuration of two vortex rings placed symmetrically on two tilted planes. The Hamiltonian structure of the inviscid limit of the model is obtained. The associated noncanonical Poisson bracket [3] and two invariants, one that serves as the Hamiltonian and the other a Casimir invariant, are discovered. It is shown that the system is integrable with a solution that lies on the intersection for the two invariants, just as for the free rigid body of mechanics whose solution lies on the intersection of the kinetic energy and angular momentum surfaces. Also, a direct quadrature is given and used to demonstrate the Leray form for finite-time singularity in the model. To the extent the Moffat and Kimura model accurately represents Euler's ideal fluid equations of motion, we have shown the existence of finite-time singularity.

---

\* [morrison@physics.utexas.edu](mailto:morrison@physics.utexas.edu)

## CONTENTS

I. Introduction	2
II. The Moffatt-Kimura system	3
III. Hamiltonian Structure	5
A. Generalities	5
B. The Hamiltonian and Poisson bracket	7
C. The Casimir Invariant	10
IV. The nature of the solution, reduction to quadrature, and analysis	12
A. Geometrical solution	12
B. Reduction to quadrature	16
C. Exact solutions with Leray scaling	19
D. General analysis	22
V. Conclusions	24
Acknowledgment	24
A. Non-Hamiltonian spectrum	25
B. The Leray Hamiltonian	26
C. Using $\kappa$ as a clock	27
References	28

## I. INTRODUCTION

One approach to the pedigreed quest for determining the existence or nonexistence of finite-time singularity in the Euler and Navier-Stokes equations of fluid dynamics (see, e.g., [4] for an overview) is to analyze them with very specialized initial conditions. Because the vorticity at a singularity must diverge [5], effort has been spent on understanding the behavior of interacting localized de-singularized vortex tubes, leading to the study of vor-

tex reconnection and its role in turbulence. Various configurations have been proposed and investigated numerically for reconnection in classical turbulence (e.g., [6–8]), quantum turbulence (e.g., [9–11]), and for the existence of singularity (e.g., [12–16]).

The present work investigates the reduced model of Moffatt and Kimura [1, 2] that describes the interaction of two circular vortex rings. To the extent this model accurately represents Euler’s ideal fluid equations of motion, we have shown the existence of finite-time singularity. Explicitly, we have shown that within the proposed limits of applicability of this model there exist solutions that blow up in finite time.

Section II describes the Moffatt and Kimura (MK) model. This is followed by Sec. III where the Hamiltonian structure of the MK model is given, which is essential for our analysis. Here we discover two constants of motion for the MK model. One invariant serves as the Hamiltonian for its noncanonical Hamiltonian formulation (flow on a Poisson manifold; see [3]), while the other turns out to be a Casimir invariant. The Hamiltonian formulation allows us, in Sec. IV, to obtain geometrical intuition about the solution space by examining the intersection of the level sets of the two invariants, akin to the visualization afforded by the constancy of the energy and angular momentum magnitude for the Euler equations that describe the free rigid body. Also in this section we show how to reduce the MK system to quadrature and obtain for special initial conditions explicit solutions that have exact Leray scaling, which is representative of the finite-time singularity. Conditions for singularity within the range of applicability of the derivation given in Refs. [1, 2] are presented. In Sec. V we summarize our results and mention some future avenues. Appendices are provided that exhibit additional features of our results.

## II. THE MOFFATT-KIMURA SYSTEM

The MK system is a three-dimensional system of ordinary differential equations that describes the evolution of two initially circular vortices of radius  $R$  and circulations  $\pm\Gamma$ , located symmetrically on planes  $x = \pm z \tan \alpha$ , with pitch angle  $\alpha$ , in an  $(x, y, z)$  Cartesian coordinate system. The system is written in dimensionless form using the space scale  $R$ , time scale  $R^2/\Gamma$ , and effective Reynolds number  $R_\Gamma = \Gamma/\nu =: 1/\varepsilon \gg 1$ . Here  $\nu$  is the usual kinematic viscosity of the fluid. It is assumed that the vortices have Gaussian cores of radius measured by  $\delta$ , a separation measured by  $s$ , and a curvature given by  $\kappa$ , which evolve

in terms of the dimensionless time according to

$$(\dot{\delta}^2) = \varepsilon - c_2 \frac{\kappa \delta^2}{s}, \quad (1)$$

$$\dot{s} = -c_2 \kappa \left[ \ln \left( \frac{s}{\delta} \right) + \beta_1 \right] \quad (2)$$

$$\dot{\kappa} = c_1 \frac{\kappa}{s^2}, \quad (3)$$

subject to the inequality constraints for applicability

$$\delta < s < 1/\kappa, \quad (4)$$

which are assumed in the derivation. Roughly speaking, these inequalities assure that the vortex cores, with size measured by  $\delta$ , are small enough so that cores do not overlap as the rings merge, i.e., as their separation given by  $s$  decreases, and that portions of the rings are sufficiently far away, as measured by  $1/\kappa$ , to allow far field expansion. The constants appearing in Eqs. (1), (2), and (3) are given by

$$c_1 = \frac{\cos \alpha \sin \alpha}{4\pi} \quad \text{and} \quad c_2 = \frac{\cos \alpha}{4\pi}, \quad (5)$$

and the parameter  $\beta_1$  depends on the vortex core, with the value  $\beta_1 = 0.4417$  for a gaussian core profile.

If the MK system is to be a reduction that inherits the noncanonical Hamiltonian structure of Euler's fluid equations (see e.g. [3]) then it will have a Hamiltonian form upon setting the  $\varepsilon = 0$ . Thus we investigate

$$\dot{\delta} = -\frac{c_2}{2} \frac{\kappa \delta}{s} \quad (6)$$

$$\dot{s} = -c_2 \kappa \left[ \ln \left( \frac{s}{\delta} \right) + \beta_1 \right] \quad (7)$$

$$\dot{\kappa} = c_1 \frac{\kappa}{s^2}. \quad (8)$$

For later use we record here the equation of motion for  $x := s/\delta$ ,

$$\dot{x} = -\frac{c_2 \kappa}{\delta} (\Lambda - 1/2), \quad (9)$$

which is easily verified. Here, for convenience, we have defined

$$\Lambda := \ln \left( \frac{s}{\delta} \right) + \beta_1 = \ln(x) + \beta_1. \quad (10)$$

The smallest value of  $\Lambda$  consistent with inequality (4) occurs when  $\delta = s$ ; thus,

$$\Lambda \geq \beta_1 \quad \text{or} \quad \Lambda - 1/2 \geq \beta_1 - 1/2 = -0.0583, \quad (11)$$

where the gaussian value of  $\beta_1 = 0.4417$  is used in the second expression. We note here that

$$\Lambda = 1/2 \quad \text{at} \quad x^* = e^{1/2-\beta_1} \approx 1.0600. \quad (12)$$

### III. HAMILTONIAN STRUCTURE

#### A. Generalities

Hamiltonian systems are usually written in terms of canonically conjugate sets of variables, a configuration space coordinate and its conjugate momentum. The noncanonical Hamiltonian description is one where the form in terms of canonical variables is not necessary and replaced by algebraic properties of the Poisson bracket. The terminology noncanonical Hamiltonian was introduced in the context of the ideal fluid and magnetohydrodynamics in [17], but the ideas date back to the work of Sophus Lie. (See, e.g., [3, 18, 19] for review.)

Given an  $n$ -dimensional phase space with coordinates  $z = (z^1, z^2, \dots, z^n)$ , a system of ordinary differential equations has noncanonical Hamiltonian form if there exists a Poisson bivector  $J$ , an antisymmetric second rank contravariant tensor, and a conserved phase space function  $H(z)$  such that the equations can be written as follows:

$$\dot{z}^i = \{z^i, H\} = J^{ij} \frac{\partial H}{\partial z^j} \quad i, j = 1, 2, \dots, n, \quad (13)$$

where repeated indices are summed and the Poisson bracket defined on functions of the coordinate  $z$ ,

$$\{f, g\} = \frac{\partial f}{\partial z^i} J^{ij} \frac{\partial g}{\partial z^j} \quad (14)$$

is bilinear, antisymmetric, and most importantly satisfies the Jacobi identity,

$$\{f, \{g, h\}\} + \{g, \{h, f\}\} + \{h, \{f, g\}\} = 0, \quad (15)$$

for all functions  $f, g, h$ . Unlike for the canonical description, the tensor  $J$ , the Poisson tensor, may depend on the coordinate  $z$ . It generates the Hamiltonian vector field as depicted on the righthand side of the second equality of (13). In coordinates, (15) is equivalent to the vanishing of the following purely antisymmetric three-tensor:

$$S^{ijk} = J^{i\ell} \frac{\partial J^{jk}}{\partial z^\ell} + J^{j\ell} \frac{\partial J^{ki}}{\partial z^\ell} + J^{k\ell} \frac{\partial J^{ij}}{\partial z^\ell} \equiv 0, \quad (16)$$

a quantity that is checked in practice.

When  $\det J \neq 0$ , an old theorem of Darboux, based on the algebraic properties of the Poisson bracket, implies that there is a coordinate change from the noncanonical coordinates  $z$  to a set of canonically conjugate coordinates. However, when  $\det J = 0$  this is not possible because of degeneracy, i.e., the existence of special functions  $C$ , called Casimir invariants, that satisfy  $\{C, f\} = 0$  for all phase space functions  $f$ . Thus, Casimir invariants are built-in to the phase space, for they will be conserved by a system generated by any Hamiltonian function. In the coordinates  $z$ ,  $C$  is a Casimir invariant if it satisfies

$$J^{ij} \frac{\partial C}{\partial z^j} = 0. \quad (17)$$

Noncanonical Hamiltonian systems possess the rich geometrical structure of so-called Poisson manifolds, where through every point of the phase space manifold is a conserved canonical Hamiltonian subspace, i.e., the manifold is foliated by symplectic leaves (see, e.g., the seminal reference [20] and the recent contribution [21]). We will see in practical terms how an interesting Poisson manifold emerges from the MK system.

For three-dimensional systems, like the MK system, the Poisson tensor  $J$  has the form

$$J = \begin{bmatrix} 0 & V_3 & -V_2 \\ -V_3 & 0 & V_1 \\ V_2 & -V_1 & 0 \end{bmatrix} \quad (18)$$

for some vector  $\mathbf{V}(z) = (V_1, V_2, V_3)$ , and it can be shown easily that (15), for the Jacobi identity, is satisfied if  $\mathbf{V}(z)$  satisfies

$$\mathbf{V} \cdot \nabla \times \mathbf{V} = 0. \quad (19)$$

Thus, for three-dimensional systems there is a convenient way to check the Jacobi identity. Because antisymmetric matrices have even rank,  $J$  must have rank 2 or 0. The latter of course would generate trivial dynamics – of interest is the case of rank 2 where there is a single Casimir invariant, and condition (17) can be written compactly as

$$\mathbf{V} \times \nabla C = 0. \quad (20)$$

Relations (19) and (20) play central roles in our discovery of the Hamiltonian structure of the MK system.

## B. The Hamiltonian and Poisson bracket

Given the equations of motion of a system, like (6), (7), and (8), and a constant of motion, one can seek a Poisson tensor by matching to the equations of motion while enforcing the Jacobi identity. Thus we seek a suitable invariant, one that physically we expect to be an energy-like quantity. Using the structure of the MK system and some insight we find (6), (7), and (8) conserve the following:

$$H = \frac{1}{\delta^2} \left[ \ln \left( \frac{s}{\delta} \right) + \beta_1 - \frac{1}{2} \right] = \frac{1}{\delta^2} [\Lambda - 1/2], \quad (21)$$

which can be shown directly. From (21) we obtain

$$s = \delta e^{\delta^2 H - \beta_1 + 1/2}. \quad (22)$$

Again, as with (11), the threshold for inequality (4) occurs when  $\delta = s$ , yielding

$$H > (\beta_1 - 1/2)/\delta^2 = -0.0583/\delta^2, \quad (23)$$

where again the gaussian value of  $\beta_1$  is used in the equality.

In terms of the coordinates  $z = (\delta, s, \kappa)$ , the analog of equation (13) for the MK system takes the form

$$\begin{bmatrix} \dot{\delta} \\ \dot{s} \\ \dot{\kappa} \end{bmatrix} = \begin{bmatrix} 0 & V_3 & -V_2 \\ -V_3 & 0 & V_1 \\ V_2 & -V_1 & 0 \end{bmatrix} \begin{bmatrix} \partial H / \partial \delta \\ \partial H / \partial s \\ \partial H / \partial \kappa \end{bmatrix}, \quad (24)$$

which upon making use of the MK equations of motion (6), (7), and (8), and the candidate Hamiltonian (21), we obtain the following equation for the Poisson tensor:

$$\begin{bmatrix} -c_2 \delta \kappa / (2s) \\ -c_2 \kappa \Lambda \\ c_1 \kappa / s^2 \end{bmatrix} = \begin{bmatrix} 0 & V_3 & -V_2 \\ -V_3 & 0 & V_1 \\ V_2 & -V_1 & 0 \end{bmatrix} \begin{bmatrix} -2\Lambda / \delta^3 \\ 1 / (s\delta^2) \\ 0 \end{bmatrix}. \quad (25)$$

Thus, the goal is to solve (25) for a  $\mathbf{V} = (V_1, V_2, V_3)$  that satisfies (19).

It follows immediately from (25) that

$$\dot{\delta} = -c_2 \delta \kappa / (2s) = V_3 / (s\delta^2) \quad \text{and} \quad \dot{s} = -c_2 \kappa \Lambda = 2V_3 \Lambda / \delta^3; \quad (26)$$

thus,

$$V_3 = -c_2 \kappa \delta^3 / 2 \quad (27)$$

works for both equations of (26). The remaining equation yields the expression,

$$\dot{\kappa} = c_1 \kappa / s^2 = -2V_2 \Lambda / \delta^3 - V_1 / (s \delta^2). \quad (28)$$

Thus, it appears there is freedom in the choices of  $V_1$  and  $V_2$  to satisfy (19), the Jacobi identity. Upon setting

$$V_1 = -c_1 \kappa \delta^2 / s - 2V_2 \Lambda s / \delta. \quad (29)$$

we seek to find a  $V_2$  that ensures (19) is satisfied. A direct calculation implies

$$\begin{aligned} \mathbf{V} \cdot \nabla \times \mathbf{V} = & -\frac{c_2}{2} \kappa \delta^3 \frac{\partial V_2}{\partial \delta} - c_2 \kappa s \delta^2 \Lambda \frac{\partial V_2}{\partial s} + c_1 \frac{\kappa \delta^2}{s} \frac{\partial V_2}{\partial \kappa} \\ & + V_2 \left( -c_1 \frac{\delta^2}{s} + \frac{c_2}{2} \kappa \delta^2 - c_2 \kappa \delta^2 \Lambda \right) + \frac{c_1 c_2}{2} \frac{\delta^5 \kappa^2}{s^2}. \end{aligned} \quad (30)$$

and the goal is to find a  $V_2$  such that (30) vanishes.

Upon inserting the following into (30),

$$V_2 = \kappa \delta A(x), \quad (31)$$

where recall  $x := s/\delta$  and using

$$\partial_k V_2 = \delta A(x), \quad \partial_s V_2 = \kappa A'(x), \quad \partial_\delta V_2 = \kappa A(x) - \kappa x A'(x) \quad (32)$$

(30) becomes

$$\mathbf{V} \cdot \nabla \times \mathbf{V} = -c_2 \kappa^2 \delta^3 \left[ x A' \left( \Lambda - \frac{1}{2} \right) + \Lambda A - \frac{c_1}{2x^2} \right]. \quad (33)$$

Thus, the Jacobi identity is satisfied provided we can find a solution  $A(x)$  to

$$x A' \left( \Lambda - \frac{1}{2} \right) + \Lambda A - \frac{c_1}{2x^2} = 0, \quad (34)$$

where recall  $\Lambda(x)$  is given by (10). If such a function  $A$  is found, then the MK system is Hamiltonian with a bracket defined by

$$V_1 = -c_1 \frac{\kappa \delta^2}{s} - 2\kappa \Lambda s A(x), \quad V_2 = \kappa \delta A(x), \quad \text{and} \quad V_3 = -\frac{c_2}{2} \kappa \delta^3. \quad (35)$$

Thus, we proceed to solve for  $A$ . In the light of the inequality (4),  $\Lambda$  is seen to be a positive monotonic function with the inverse

$$x = e^{\Lambda - \beta_1}. \quad (36)$$



Consequently, we can use  $\Lambda$  as the independent variable and rewrite (34) as

$$\frac{d}{d\Lambda} \left( e^\Lambda \sqrt{\Lambda - 1/2} A \right) = \frac{c_1}{2x^2} \frac{e^\Lambda}{\sqrt{\Lambda - 1/2}} = \frac{c_1 e^{2\beta_1}}{2} \frac{e^{-\Lambda}}{\sqrt{\Lambda - 1/2}}. \quad (37)$$

Here we have assumed  $\Lambda - 1/2 \geq 0$ . In light of (11) this may not be true; thus, we will return and consider the case where  $\Lambda - 1/2 \leq 0$ .

Antidifferentiating both sides gives

$$A = \frac{e^{-\Lambda}}{\sqrt{\Lambda - 1/2}} \frac{c_1 e^{2\beta_1 - 1/2}}{2} \int^{\Lambda - 1/2} \frac{e^{-\ell}}{\sqrt{\ell}} d\ell. \quad (38)$$

Then, with the definition of the incomplete gamma function

$$\gamma(\sigma, u) = \int_0^u u'^{\sigma-1} e^{-u'} du', \quad (39)$$

and the identity

$$\gamma(1/2, u) = \sqrt{\pi} \operatorname{erf}(\sqrt{u}) = 2 \int_0^{\sqrt{u}} e^{-u'^2} du', \quad (40)$$

with  $\operatorname{erf}$  being the error function, we obtain

$$A = c_0 \frac{e^{-\Lambda}}{\sqrt{\Lambda - 1/2}} + \frac{\sqrt{\pi} c_1}{2} e^{2\beta_1 - 1/2} \frac{e^{-\Lambda}}{\sqrt{\Lambda - 1/2}} \operatorname{erf} \left( \sqrt{\Lambda - 1/2} \right), \quad (41)$$

where  $c_0 \in \mathbb{R}$  is the integration constant. Upon inserting (41) into the expressions of (35), we have a one-parameter family of Poisson brackets. It is convenient to choose  $c_0 = 0$ , giving

$$A = \frac{\sqrt{\pi} c_1}{2x} \frac{e^{\beta_1 - 1/2}}{\sqrt{\Lambda - 1/2}} \operatorname{erf} \left( \sqrt{\Lambda - 1/2} \right), \quad (42)$$

which is valid for  $\Lambda - 1/2 \geq 0$ , but we will see it is also valid for  $\Lambda - 1/2 < 0$ . Observe, the choice  $c_0 = 0$  gives us regularity at  $\Lambda = 1/2$ . Inserting (42) into the equations of (35) defines the noncanonical Poisson bracket that we will use for  $\Lambda \geq 1/2$ .

Now consider the case where  $\Lambda \leq 1/2$ , which occurs for

$$0 \leq 1/2 - \Lambda \leq 1/2 - \beta_1 - \ln x \leq 1/2 - \beta_1, \quad (43)$$

where we assume  $x \geq 1$  consistent again with (4). Instead of (37), consider

$$\frac{d}{d\Lambda} \left( e^\Lambda \sqrt{1/2 - \Lambda} A \right) = -\frac{c_1 e^{2\beta_1}}{2} \frac{e^{-\Lambda}}{\sqrt{1/2 - \Lambda}}, \quad (44)$$

where (34) has been used. Integrating both sides from  $\Lambda = 1/2$  leads to

$$A = c_1 e^{2\beta_1 - 1/2} e^{-\Lambda} M(1/2, 3/2, 1/2 - \Lambda), \quad \Lambda \leq 1/2, \quad (45)$$

where

$$M(1/2, 3/2, z) = \frac{1}{2} \int_0^1 \frac{e^{zt}}{\sqrt{t}} dt = \frac{1}{2\sqrt{z}} \int_0^z \frac{e^u}{\sqrt{u}} du, \quad (46)$$

is the Kummer function [22], which is sometimes called the confluent hypergeometric function of the first kind and denoted by  ${}_1F_1(1/2; 3/2; z)$ . Inserting (45) into the equations of (35) defines the noncanonical Poisson bracket defined for  $\beta_1 \leq \Lambda \leq 1/2$ .

A comparison of (42) and (45) follows from the identity

$$\operatorname{erf}(z) = \frac{2z}{\sqrt{\pi}} M(1/2, 3/2, -z^2), \quad (47)$$

which implies

$$\frac{\sqrt{\pi}}{2} \frac{1}{\sqrt{\Lambda - 1/2}} \operatorname{erf}\left(\sqrt{\Lambda - 1/2}\right) = M(1/2, 3/2, 1/2 - \Lambda). \quad (48)$$

Because  $\operatorname{erf}(ix)$  for  $x \in \mathbb{R}$  is pure imaginary, like  $\sqrt{\Lambda - 1/2}$  for  $\Lambda < 1/2$ , we can analytically continue the expression in terms of the error function through zero to pure imaginary values yielding a real quantity. Thus, expression (42) can be used for both  $\Lambda \geq 0$  and  $\Lambda < 0$ .

### C. The Casimir Invariant

Given the Hamiltonian structure of Sec. III B we know immediately that the MK system must possess another constant of motion, the Casimir invariant. A little thought reveals the Casimir must have the form

$$C = \frac{c_2}{2} \kappa + \frac{\lambda(x)}{\delta}. \quad (49)$$

In the present context, (20) is equivalent to

$$\begin{bmatrix} 0 & V_3 & -V_2 \\ -V_3 & 0 & V_1 \\ V_2 & -V_1 & 0 \end{bmatrix} \begin{bmatrix} \partial C / \partial \delta \\ \partial C / \partial s \\ \partial C / \partial \kappa \end{bmatrix} = \begin{bmatrix} 0 & V_3 & -V_2 \\ -V_3 & 0 & V_1 \\ V_2 & -V_1 & 0 \end{bmatrix} \begin{bmatrix} -\lambda / \delta^2 - s \lambda' / \delta^3 \\ \lambda' / \delta^2 \\ c_2 / 2 \end{bmatrix} = 0 \quad (50)$$

The first equation gives

$$0 = -\frac{c_2}{2} \kappa \delta^3 \frac{\lambda'}{\delta^2} - \kappa \delta A \frac{c_2}{2} \Rightarrow \lambda' = -A, \quad (51)$$

while the second gives after some manipulation

$$0 = -\frac{c_2 \kappa \delta}{2} \left( \lambda - x A + \frac{c_1}{x} + 2 A x \Lambda \right). \quad (52)$$

Because of the Jacobi identity, the third equation must automatically be solved by the above, which can be verified directly. Thus we have

$$\lambda'(x) = -A(x) \quad (53)$$

$$\lambda(x) = Ax(1 - 2\Lambda) - \frac{c_1}{x} = -2Ax(\Lambda - 1/2) - \frac{c_1}{x}, \quad (54)$$

where  $A$  solves (34). Upon differentiating (54) we see that if  $A$  satisfies (34), then (53) is automatic for a solution of (54). In particular, using (42) we obtain

$$\lambda(x) = -\sqrt{\pi}c_1 e^{\beta_1-1/2} \sqrt{\Lambda - 1/2} \operatorname{erf}\left(\sqrt{\Lambda - 1/2}\right) - \frac{c_1}{x}, \quad (55)$$

where use has been made of  $xe^{-\Lambda} = e^{-\beta_1}$ . Figure 1 displays plots of both  $A/c_1$  of (42) (upper) and  $\lambda/c_1$  (55) (lower) as functions of  $x$ , beginning with its critical value of  $x = s/\delta = 1$ , revealing that both are relatively simple monotonic functions consistent with inequality (4).

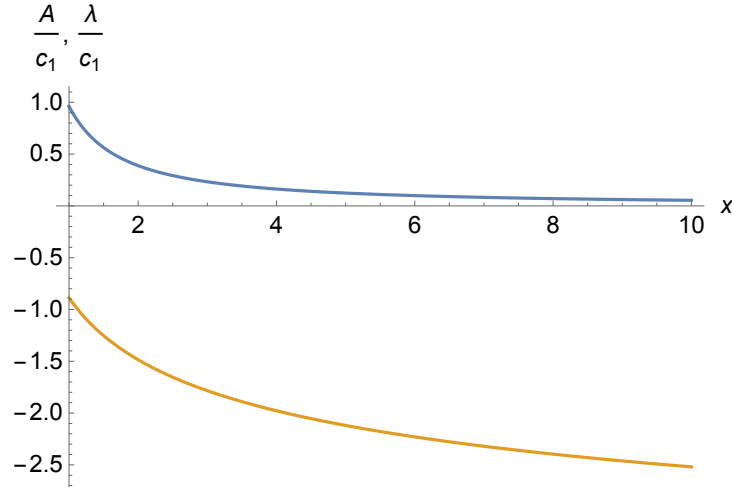


FIG. 1. Plots of  $A/c_1$  (blue) and  $\lambda/c_1$  (orange) vs.  $x = s/\delta$ . Recall  $\lambda' = -A(x)$  [cf. Eq. (53)].

Thus to summarize, the Casimir, a second invariant, is given by

$$\begin{aligned} C &= \frac{c_2}{2}\kappa + \frac{\lambda(x)}{\delta} \\ &= \frac{c_2}{2}\kappa - \sqrt{\pi}c_1 e^{\beta_1-1/2} \frac{1}{\delta} \sqrt{\Lambda - 1/2} \operatorname{erf}\left(\sqrt{\Lambda - 1/2}\right) - \frac{c_1}{s}, \end{aligned} \quad (56)$$

where we have inserted  $\lambda$  from (55) in (56) and used  $x = s/\delta$ . We remind the reader that (56) is valid for  $\Lambda < 1/2$  as well as for  $\Lambda \geq 1/2$ .

Because of inequality (4), not all values of (56) are permissible. To understand the permissible range, we rewrite (56) as follows:

$$\frac{s}{c_1}C - \frac{c_2}{2c_1}\kappa s = F(\Lambda), \quad (57)$$

where

$$F(\Lambda) = \sqrt{\pi} e^{\Lambda-1/2} \sqrt{\Lambda - 1/2} \operatorname{erf} \left( \sqrt{\Lambda - 1/2} \right) + 1 > 0. \quad (58)$$

As noted in (11), the smallest allowable value of  $\Lambda$  is  $\beta_1$ , and it is not hard to show that  $F(\Lambda)$  obtains its minimum value at  $\beta_1$ , at which it is positive. Thus we see, the Casimir must satisfy

$$C < \frac{c_2}{2}\kappa \quad (59)$$

to be consistent with the inequality (4).

#### IV. THE NATURE OF THE SOLUTION, REDUCTION TO QUADRATURE, AND ANALYSIS

##### A. Geometrical solution

Given that we have a three-dimensional system with two constants of motion, the solution space can be visualized by examining the intersection of the level sets of the Hamiltonian  $H$  of (21) with those of the Casimir  $C$  of (56). This is a direct analog of how the stable and unstable trajectories of the free rigid body, as governed by Euler's equations, are understood in terms of the intersection of the angular momentum spheres with the energy ellipsoids. The same situation occurs for other noncanonical Hamiltonian systems such as the Kida problem of fluid mechanics [23] and the rattleback toy [24], and indeed a large class of flows on Poisson manifolds [21]. Thus, by plotting level sets of (21) and (56) the nature of trajectories is revealed and, in addition, one can delineate the accessible phase space consistent with (4).

Figure 2 displays contours of the Hamiltonian  $H$  of (21). Since  $H$  is independent of the variable  $\kappa$  it has translational symmetry along the  $\kappa$  axis and, as can be seen in Fig. 2(a), has a sheet-like topology for positive values of the variables. Level sets corresponding to different signs of  $H$  have opposite curvature in the  $s - \delta$  plane, with there being a region of negative values of  $H$  consistent with (23) and (4). This ‘negative energy’ interval is shown

in Fig. 2(b) for  $\delta < 1$ . For all values of  $H$ , the sheets become tangent to the  $H = 0$  plane with a slope given by  $s = \delta e^{1/2 - \beta_1}$ . Consequently, if  $\delta$  and  $s$  approach zero, they do so in a clear and universal way independent of  $\dot{H}$ , the initial value of the Hamiltonian constant of motion.

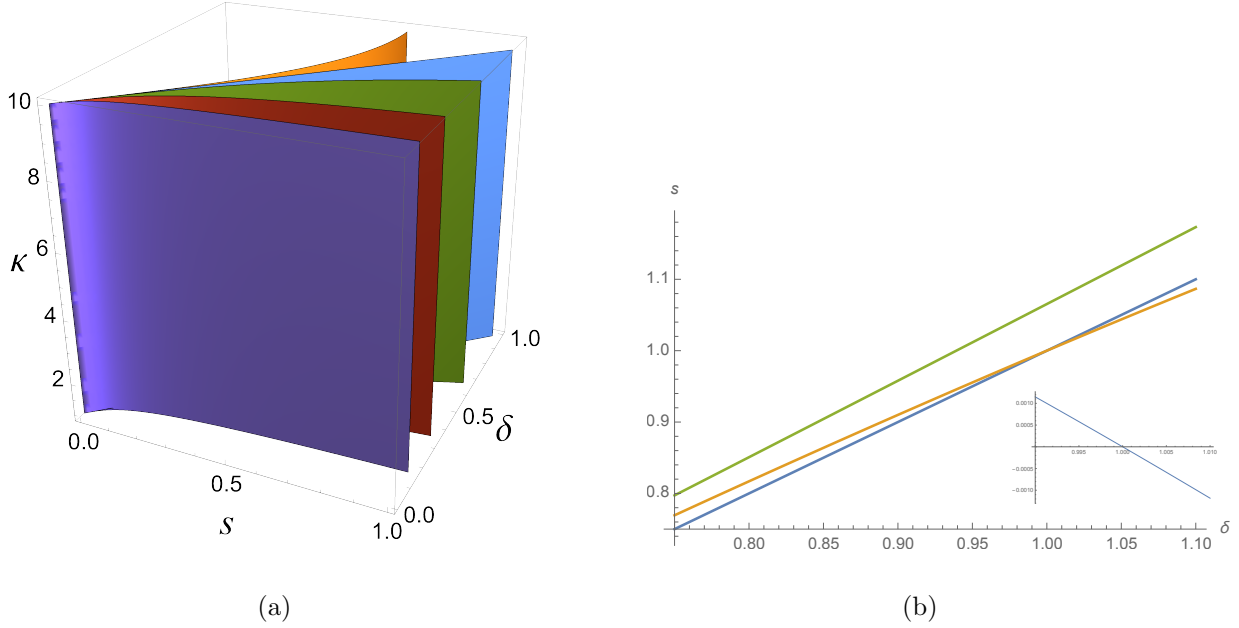


FIG. 2. Contour plots of the Hamiltonian  $H$  of (21). (a)  $\dot{H} = -0.50$  (orange),  $\dot{H} = 0$  (blue),  $\dot{H} = 1$  (green),  $\dot{H} = 10$  (magenta), and  $\dot{H} = 100$  (lavender). (b) Closeup plots of  $s$  vs.  $\delta$  at arbitrary  $\kappa$ . Note the region to the left of  $\delta = 1$  for the case where  $\dot{H} = -0.0583$  (orange) compared to the case  $s = \delta$  (blue) with the inset showing the difference (orange-blue), showing that  $s > \delta$  to the left. The other curve with  $\dot{H} = 0.005$  (green) is added for comparison.

In Figs. 3, 4, and 5 we show two views of contour plots of the Casimir of (56) for three values of the vortex ring tilt angle  $\alpha \in \{\pi/4, \pi/6, \pi/90\}$ . Observe that these surfaces are again sheet like but with more interesting structure, no longer having the  $\kappa$  independence of the  $H$ -surfaces.

The case where  $\alpha = \pi/90$  corresponds to nearly parallel vortices. For this case  $c_1 \approx 5 \times 10^{-5} \ll 1$  and (3) implies  $\kappa$  is nearly constant. For this case the trajectory lingers in the flat regions of Fig. 5 and the dynamics is approximately governed by

$$\dot{\delta} = -\frac{c_2}{2} \frac{\kappa \delta}{s} \quad (60)$$

$$\dot{s} = -c_2 \kappa \left[ \ln \left( \frac{s}{\delta} \right) + \beta_1 \right], \quad (61)$$

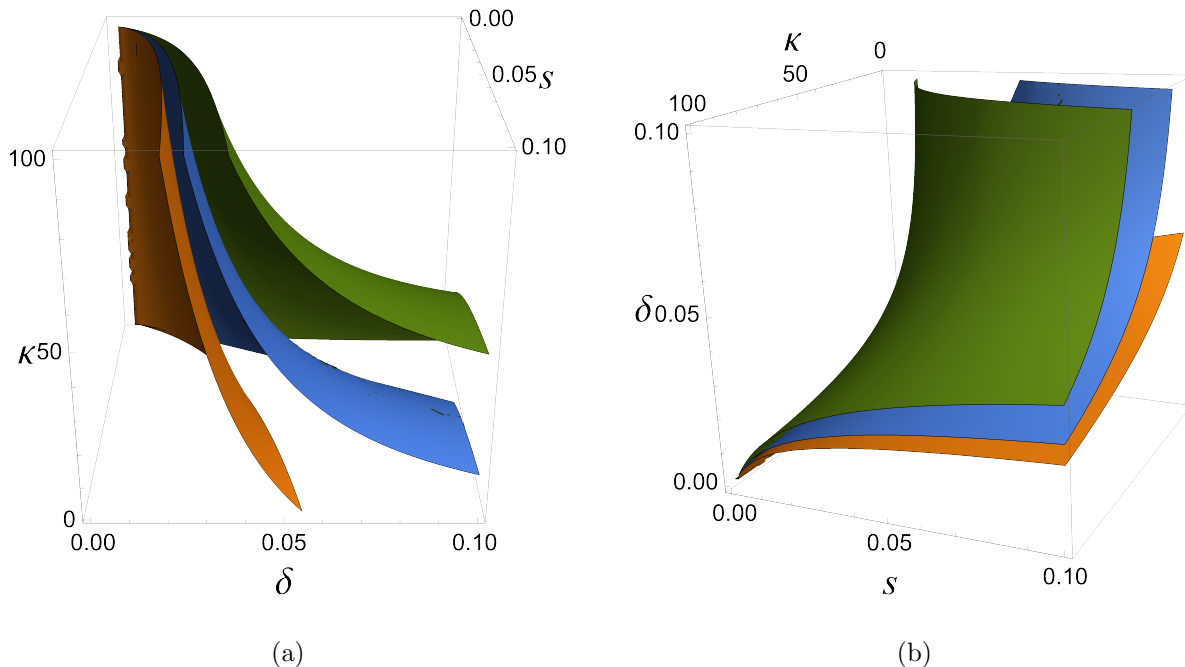


FIG. 3. (a) View of the level sets of the Casimir  $C$  for  $\alpha = \pi/4$ . (b) Same as (a) but rotated.

with  $c_2 \approx 0.0796$ . Because  $H$  is independent of  $\kappa$ , it is not a surprise that (21) is still conserved by (60) and (61). This leads to the quadrature discussed in Appendix C, where the ‘ $\kappa$ -clock’ is proportional to ordinary time. As  $s$  gets small,  $\kappa$  becomes activated, demonstrating the importance of the local induction velocity for developing curvature.

Now consider the roles played by the  $H$  and  $C$  surfaces. As a specific example, consider the case with the initial conditions

$$\dot{\delta} = 0.01 < \dot{s} = 0.10 < \dot{\kappa} = 1. \quad (62)$$

With the values of (62) and a choice for the vortex ring tilt angle  $\alpha$ , the solution lies on the intersection of the level sets with

$$\dot{H} = 22442.9 \quad \text{and} \quad \dot{C} = -6.40628, \quad \text{for} \quad \alpha = \pi/9, \quad (63)$$

where again we use  $\beta_1 = 0.4417$ . Thus, these initial conditions and corresponding initial values of  $\dot{H}$  and  $\dot{C}$  are consistent with (4). This particular intersection is displayed in Fig. 6. Observe how the curve of intersection approaches increasingly large values of  $\kappa$  as both  $\delta$  and  $s$  approach zero.

In Fig. 7 we plot multiple intersections of the  $H$  and  $C$  contours. From this figure we see how  $\kappa$  diverges for a variety of initial conditions, behavior that is in fact generic.

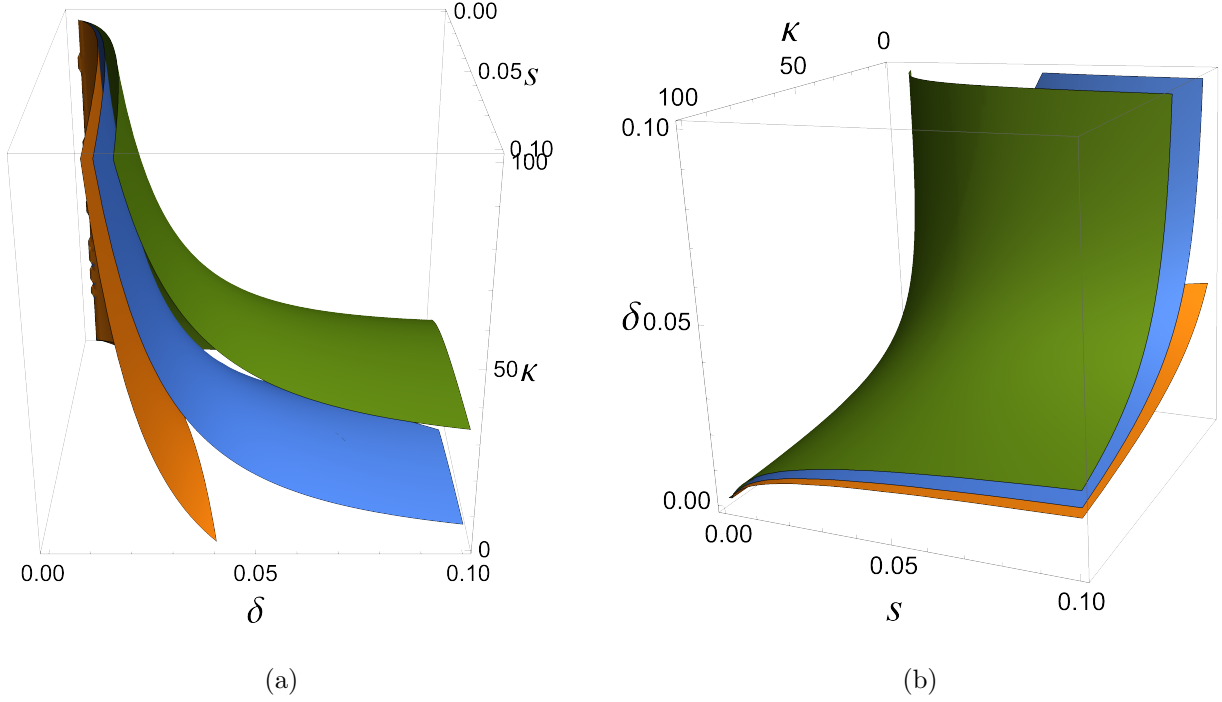


FIG. 4. (a) View of the level sets of the Casimir  $C$  for  $\alpha = \pi/9$ . (b) Same as (a) but rotated.

Yet another picture of the singularity emerges if we eliminate  $\delta$  between (21) and (56), giving the expression

$$\begin{aligned}
 \frac{c_2 \kappa}{2C} &= 1 - \frac{\sqrt{H}}{C} \frac{\lambda(x)}{\sqrt{\Lambda(x) - 1/2}} \\
 &= 1 + \frac{c_1 \sqrt{H}/C}{\sqrt{\Lambda(x) - 1/2}} \left( \sqrt{\pi} e^{\beta_1 - 1/2} \sqrt{\Lambda - 1/2} \operatorname{erf} \left( \sqrt{\Lambda - 1/2} \right) + \frac{1}{x} \right) \\
 &=: 1 + \frac{c_1 \sqrt{H}}{C} K[x].
 \end{aligned} \tag{64}$$

This formula is well defined for  $H < 0$  because  $\delta = \sqrt{H/(\Lambda - 1/2)} > 0$ . Figure 8 shows the function  $K$  with the singularity occurring at  $x^* \approx 1.0600$ .

The reader may wonder what would happen to the Casimir if we retained the term of (41) with the integration constant  $c_0$ . It turns out that this merely adds a term proportional to  $\sqrt{H}$  to the Casimir and thus just shifts the value of  $C$ , and thus has no consequence other than changing the numerical value of  $C$  for the same plots.

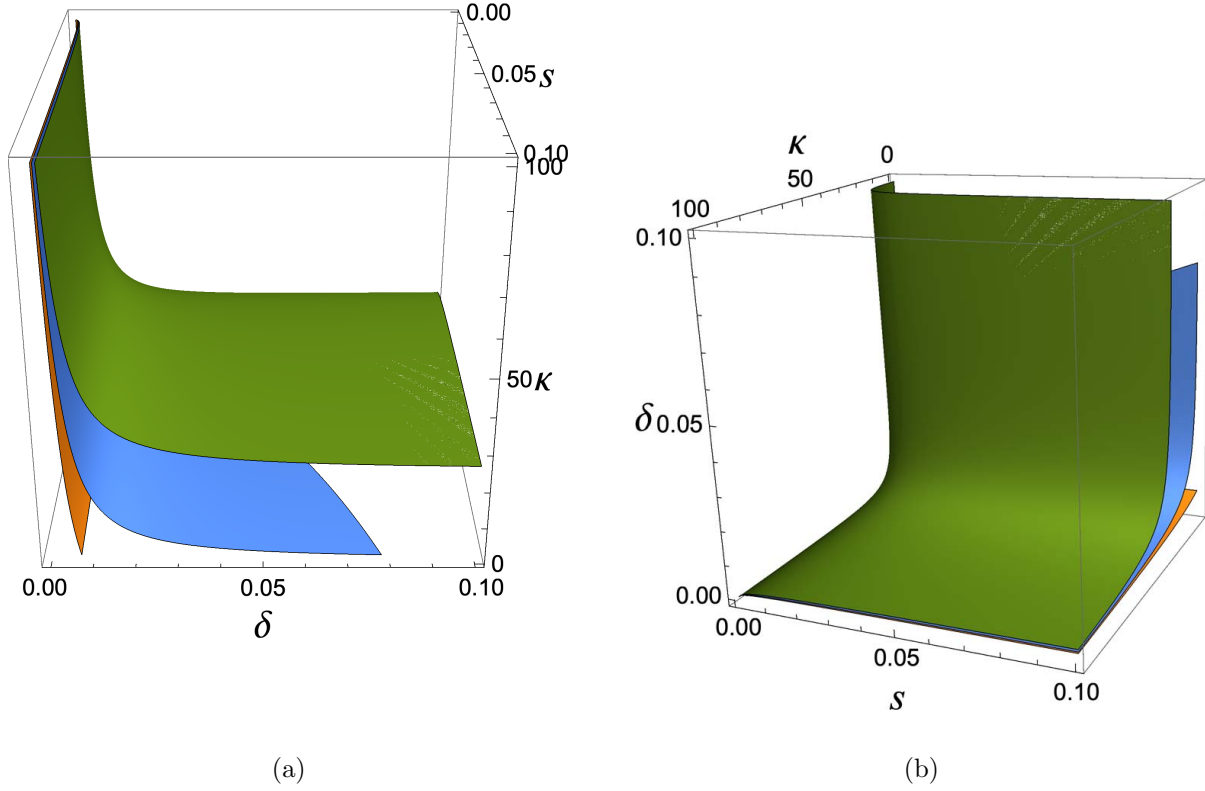


FIG. 5. (a) View of the level sets of the Casimir  $C$  for  $\alpha = \pi/90$ . (b) Same as (a) but rotated.

## B. Reduction to quadrature

Let us now consider exact integration of the system. Suppose  $(\overset{\circ}{\delta}, \overset{\circ}{s}, \overset{\circ}{\kappa})$  represent an arbitrary initial condition at time  $\overset{\circ}{t}$  with corresponding initial values of our two invariants  $\overset{\circ}{H} = H(\overset{\circ}{\delta}, \overset{\circ}{s}, \overset{\circ}{\kappa})$  and  $\overset{\circ}{C} = C(\overset{\circ}{\delta}, \overset{\circ}{s}, \overset{\circ}{\kappa})$ . Because  $H = \overset{\circ}{H}$  for all time, (21) can be used in (56) to obtain

$$\overset{\circ}{C} = \frac{c_2}{2}\kappa - c_1 e^{\beta_1 - 1/2} \sqrt{\pi \overset{\circ}{H}} \operatorname{erf}\left(\delta \sqrt{\overset{\circ}{H}}\right) - \frac{c_1}{s}, \quad (65)$$

where recall this formula is well-defined when  $\overset{\circ}{H} < 0$  because it analytically continues to the expression of (45). Next, using (22) to eliminate  $s$  we obtain

$$\overset{\circ}{C} = \frac{c_2}{2}\kappa - c_1 e^{\beta_1 - 1/2} \sqrt{\pi \overset{\circ}{H}} \operatorname{erf}\left(\delta \sqrt{\overset{\circ}{H}}\right) - \frac{c_1}{\delta} e^{-\delta^2 \overset{\circ}{H} + \beta_1 - 1/2}. \quad (66)$$

Solving (66) for  $\kappa$  is immediate

$$\frac{c_2}{2}\kappa = \overset{\circ}{C} + c_1 e^{\beta_1 - 1/2} \sqrt{\pi \overset{\circ}{H}} \operatorname{erf}\left(\delta \sqrt{\overset{\circ}{H}}\right) + \frac{c_1}{\delta} e^{-\delta^2 \overset{\circ}{H} + \beta_1 - 1/2}. \quad (67)$$



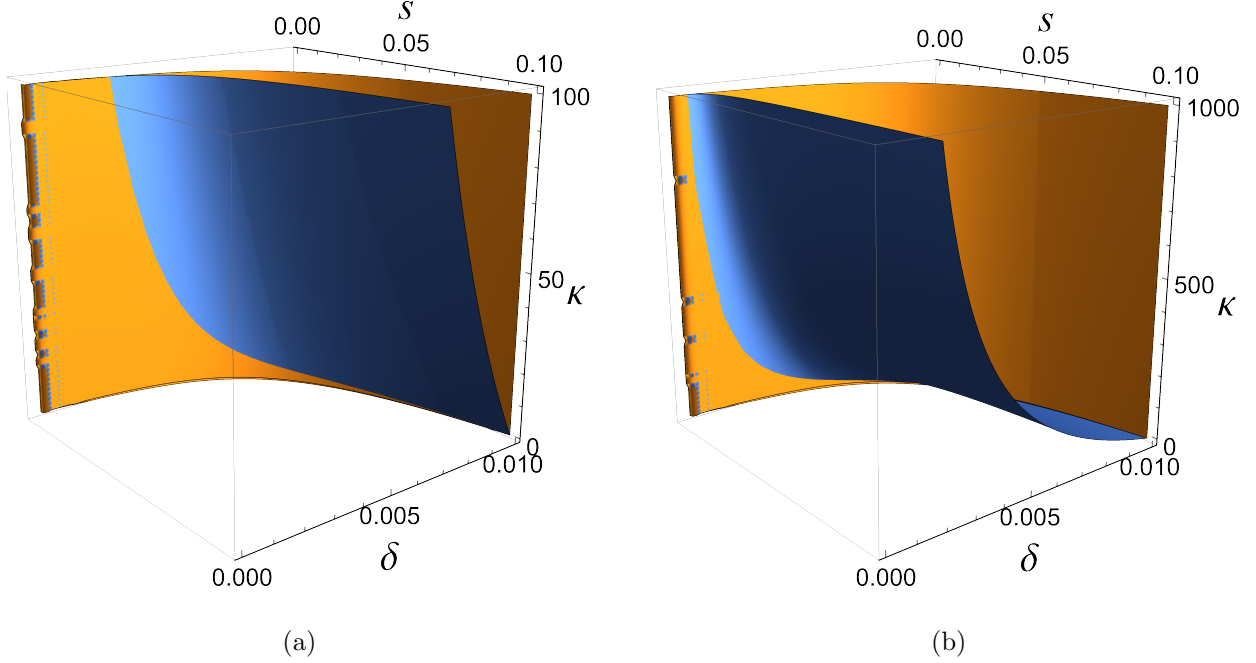


FIG. 6. Plot of the intersection of the level set  $\dot{H} = 22442.9$  (orange) with that of  $\dot{C} = -6.40628$  (blue) for  $\alpha = \pi/9$ . These values correspond to the initial conditions of (62). In (a)  $\kappa$  ranges to 100, while in (b) we zoom out to  $\kappa$  ranging to 1000 to give a more global perspective on the shape of the surfaces.

With (22) and (67), we obtain from (6), the following:

$$\begin{aligned} \dot{\delta} &= -\frac{c_2}{2} \frac{\kappa \delta}{s} = -\frac{c_2}{2} \kappa e^{-\delta^2 \dot{H} + \beta_1 - 1/2} \\ &= -\left( \dot{C} + c_1 e^{\beta_1 - 1/2} \sqrt{\pi \dot{H}} \operatorname{erf}\left(\delta \sqrt{\dot{H}}\right) + \frac{c_1}{\delta} e^{-\delta^2 \dot{H} + \beta_1 - 1/2} \right) e^{-\delta^2 \dot{H} + \beta_1 - 1/2}, \end{aligned} \quad (68)$$

which leads immediately to the quadrature

$$\dot{t} - t = e^{-2\beta_1 + 1} \int_{\dot{\delta}}^{\delta} \frac{e^{\delta'^2 \dot{H}} \delta' d\delta'}{\delta' e^{-\beta_1 + 1/2} \dot{C} + c_1 \sqrt{\pi \dot{H}} \delta' \operatorname{erf}\left(\delta' \sqrt{\dot{H}}\right) + c_1 e^{-\delta'^2 \dot{H}}}. \quad (69)$$

Although unwieldy, integration of (69) gives  $\delta$  as a function of time, and via (22) and (67) we obtain  $s$  and  $\kappa$  as functions of time, with the latter diverging.

From (69) we see that if there is a finite-time singularity where  $\delta \rightarrow 0$ , then it occurs at a time  $t_\infty$  in accordance with the following formula:

$$t_\infty = \dot{t} + e^{-2\beta_1 + 1} \int_0^{\dot{\delta}} \frac{e^{\delta'^2 \dot{H}} \delta' d\delta'}{\delta' e^{-\beta_1 + 1/2} \dot{C} + c_1 \sqrt{\pi \dot{H}} \delta' \operatorname{erf}\left(\delta' \sqrt{\dot{H}}\right) + c_1 e^{-\delta'^2 \dot{H}}}. \quad (70)$$

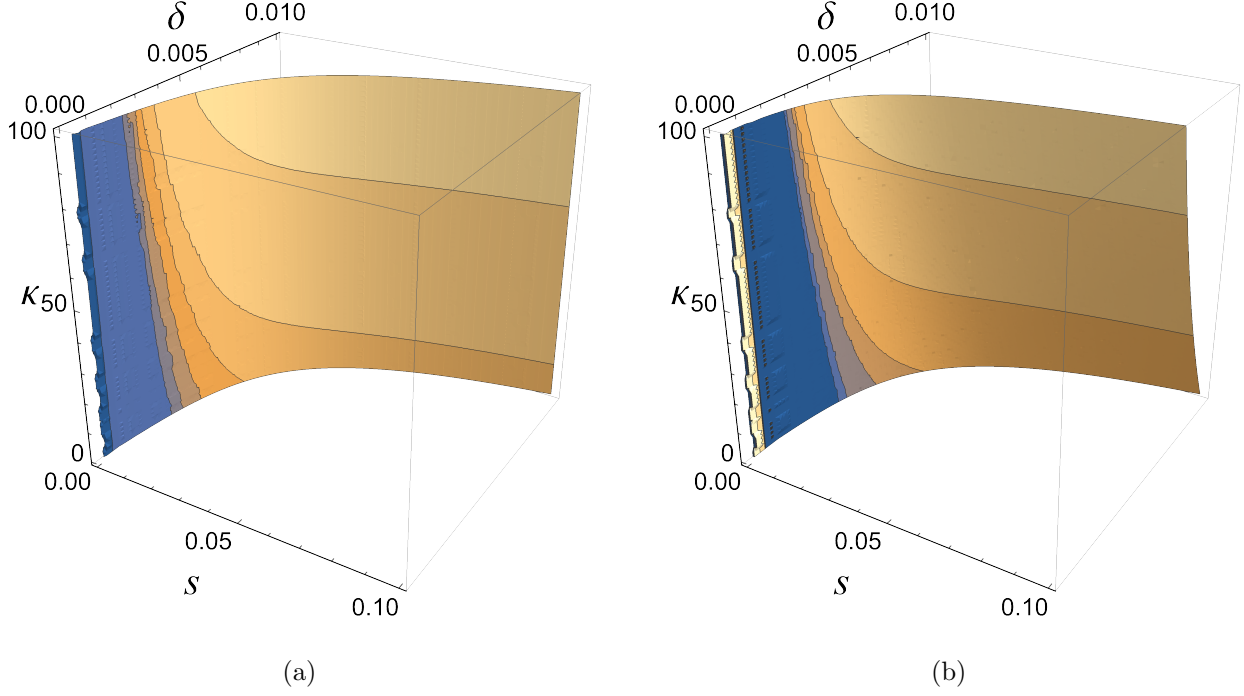


FIG. 7. Intersections of the level sets of  $H$  and  $C$  for the initial conditions of 62 with  $\alpha = \pi/9$ . In (a) we set  $\mathring{C} = -6.40628$  and show contours for  $\mathring{H} \in \{5,000; 15,000; 20,100; 30,000; 45,000\}$ , while in (b) we set  $\mathring{H} = 22442.9$  and show contours for  $\mathring{C} \in \{-10, -9, -8, -7, -6, -4\}$ .

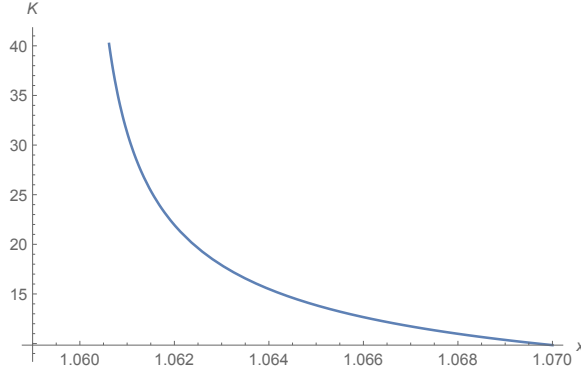


FIG. 8. Plots of the function  $K$  of (64) vs.  $x$ , depicting the singularity that occurs for  $\kappa$  at  $x^* \approx 1.0600$ .

For  $\mathring{H} \neq 0$ , we see from (21) that at a singularity where  $\delta \rightarrow 0$ , we must have  $\Lambda - 1/2 \rightarrow 0$ . As noted in (23), the smallest initial value of  $H$  that satisfies (4) is  $\mathring{H}^* = (\beta_1 - 1/2)/\mathring{\delta}^2$ , which is negative; if  $\mathring{H} > \mathring{H}^*$ , then (4) is satisfied initially. If  $\delta$  decreases and it initially satisfies  $s > \delta$ , then it will satisfy it throughout its evolution because  $\delta = s e^{-\delta^2 \mathring{H} + \beta_1 - 1/2}$ .

### C. Exact solutions with Leray scaling

Evidently, the integral of (69) is dramatically simplified with the choice  $\mathring{H} = 0$ . With this choice, (22) implies

$$s = \delta e^{-\beta_1+1/2} \quad (71)$$

and equations (6) and (7) become identical upon setting

$$\Lambda = \ln(s/\delta) + \beta_1 = 1/2,$$

a choice consistent with the inequality of (4). Given that for gaussian core profiles  $\beta_1 = 0.4417$  (see [1]), we have

$$e^{-\beta_1+1/2} = 1.0600 \quad \Rightarrow \quad s > \delta. \quad (72)$$

Thus inequality (4) is satisfied, although only barely. Proceeding, the MK system reduces for  $\mathring{H} = 0$  to

$$\dot{s} = -\frac{c_2}{2} \kappa \quad \text{and} \quad \dot{\kappa} = c_1 \frac{\kappa}{s^2}, \quad (73)$$

with the Casimir becoming

$$C = \frac{c_2}{2} \kappa - \frac{c_1}{s}, \quad (74)$$

which follows from (65).

Before considering arbitrary initial  $\mathring{C}$ , we consider the easily tractable case where both  $\mathring{H} = 0$  and  $\mathring{C} = 0$ . This implies

$$s\kappa = 2c_1/c_2 = 2 \sin \alpha. \quad (75)$$

Therefore if we choose

$$2 \sin \alpha < 1 \quad \text{or} \quad \alpha < \frac{\pi}{6}, \quad (76)$$

then the other part of the inequality (4) is satisfied, viz.  $s < 1/\kappa$ . Note, the value of  $\alpha = \pi/4$  chosen in [1, 2] does not satisfy this inequality. Using (75) in the  $\dot{\kappa}$  equation of (73) gives

$$\dot{\kappa} = \frac{c_2^2}{4c_1} \kappa^3, \quad (77)$$

which is easily integrated to obtain

$$-\frac{1}{2\kappa^2} + \frac{1}{2\dot{\kappa}^2} = \frac{c_2^2}{4c_1} (t - \mathring{t}) \quad (78)$$

and the exact solution

$$\kappa^{-1} = \sqrt{\frac{c_2^2}{2c_1}(t_\infty - t)} = \sqrt{\frac{\cot\alpha}{8\pi}(t_\infty - t)}, \quad (79)$$

where

$$t_\infty = \dot{t} + \frac{2c_1}{c_2^2 \dot{\kappa}^2} = \dot{t} + \frac{8\pi \tan\alpha}{\dot{\kappa}^2}. \quad (80)$$

As expected, smaller values of  $\kappa$  take longer to diverge.

The rest of the solution is obtained from (75) and (71), i.e.,

$$\begin{aligned} s &= 2\kappa^{-1} \sin\alpha = 2\sin\alpha \sqrt{\frac{\cot\alpha}{8\pi}(t_\infty - t)} \\ &= \sqrt{\frac{\sin(2\alpha)}{4\pi}(t_\infty - t)} = \delta e^{1/2 - \beta_1}. \end{aligned} \quad (81)$$

It is a simple matter to insert the solutions of (79) and (81) into (6), (7), and (8) to verify directly that they are indeed an exact solution, one that satisfies the inequalities of (4).

Now consider the more general case  $\dot{C} \neq 0$ . Solving (74) for  $s$  and inserting into (73) gives

$$\dot{\kappa} = \frac{\kappa}{c_1} \left( \frac{c_2}{2} \kappa - \dot{C} \right)^2 = \frac{c_2^2}{4c_1} \kappa \left( \kappa - 2\dot{C}/c_2 \right)^2, \quad (82)$$

which is easily integrated to obtain the exact solution,

$$\ln \left( 1 - \frac{2\dot{C}/c_2}{\kappa} \right) + \frac{2\dot{C}/c_2}{\kappa \left( 1 - \frac{2\dot{C}/c_2}{\kappa} \right)} - \ln \left( 1 - \frac{2\dot{C}/c_2}{\dot{\kappa}} \right) - \frac{2\dot{C}/c_2}{\dot{\kappa} \left( 1 - \frac{2\dot{C}/c_2}{\dot{\kappa}} \right)} = -\frac{\dot{C}^2}{c_1} (t - \dot{t}). \quad (83)$$

Because the model only makes sense if  $\delta$ ,  $s$ , and  $\kappa$  are all greater than or equal to zero, we must have  $c_1/s = \kappa c_2/2 - C \geq 0$  or  $1 - 2C/(\kappa c_2) \geq 0$ , which in fact according to (59) is true for all allowable values of  $\dot{H}$ .

Assuming the physical initial conditions satisfy  $\dot{\kappa} > 2\dot{C}/c_2$ , we see the  $\dot{\kappa} > 0$ , so  $\kappa$  continues to grow, with divergence occurring at the finite time

$$t_\infty = \dot{t} + \frac{c_1}{\dot{C}^2} \left( \ln \left( 1 - \frac{2\dot{C}/c_2}{\dot{\kappa}} \right) + \frac{2\dot{C}/c_2}{\dot{\kappa} \left( 1 - \frac{2\dot{C}/c_2}{\dot{\kappa}} \right)} \right), \quad (84)$$

an approximation to (70) but a generalization to (80). This is depicted in Fig. 9(a),

The quantity  $t_\infty$  can also be written as a function of  $\kappa s$ , which makes it convenient for assessing initial conditions compatible with (4). Using (74) we obtain

$$t_\infty = \dot{t} + \frac{c_1}{\dot{C}^2} \left( \ln(X) + \frac{1}{X} - 1 \right), \quad (85)$$

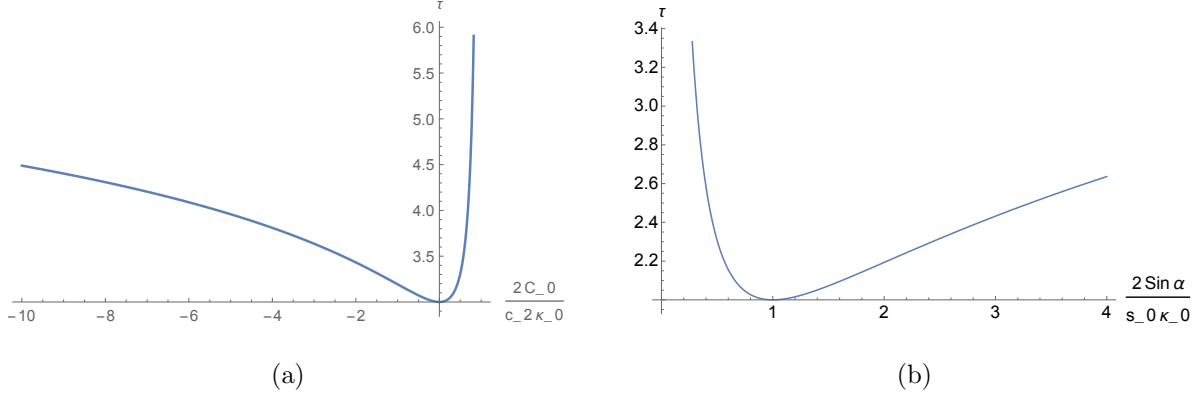


FIG. 9. Plots of the blowup times for  $\dot{H} = 0$ ,  $\dot{C} \neq 0$ , (a) according to Eq. (84) where  $\tau = (t_\infty - t)\dot{C}^2/c_1$  vs.  $2\dot{C}/(c_2\kappa)$  and (b) according to Eq. (84) where  $\tau = (t_\infty - t)\dot{C}^2/c_1$  vs.  $X = 2 \sin \alpha / (\kappa \dot{s})$ .

where

$$X = \frac{2c_1}{c_2 \kappa \dot{s}} = \frac{2 \sin \alpha}{\kappa \dot{s}}. \quad (86)$$

Observe from Fig. 9(a) there is blow up for all values of  $\dot{C}$ , but only values consistent with  $\dot{s} < 1/\kappa$  are acceptable. Thus,

$$\frac{1}{\dot{s}\kappa} > 1 \quad \Rightarrow \quad \frac{2 \sin \alpha}{\dot{s}\kappa} > 2 \sin \alpha. \quad (87)$$

Therefore after choosing  $2 \sin \alpha < 1$ , only blowup times to the right of this value in Fig. 9(b) are consistent with (4).

As for the case  $\dot{C} = 0$ , given the solution of (83) for  $\kappa$ , we immediately obtain the solutions for  $s$  and  $\delta$  from (74) and (71), respectively,

$$s = \frac{2c_1/c_2}{\kappa - 2\dot{C}/c_2} = \delta e^{-\beta_1+1/2}. \quad (88)$$

At late times, expansion of (83) again gives

$$\kappa^{-1} \sim \sqrt{\frac{c_2^2}{2c_1}(t_\infty - t)}, \quad (89)$$

in agreement with the Leray scaling suggested in [1] and proven above in (79) and (81). Note, in (79), the constant  $\dot{C}$  only appears via  $t_\infty$ . The zero energy case is special in that it is tractable, but the Leray scaling is ubiquitous. Inserting (79) into (88) we obtain for late times

$$s = \delta e^{-\beta_1+1/2} \sim \sqrt{2c_1(t_\infty - t)} \quad (90)$$

and so  $\kappa s \sim 2c_2/c_1$  as for the case with  $\dot{C} = 0$ .

## D. General analysis

Let us now return to (69) and consider the general solution. Because  $\mathring{C}$  is arbitrary, it follows immediately from (68) that there is a family of equilibrium points of  $\delta$  when the righthand side vanishes. However, by (67), all of these correspond to  $\kappa = 0$  (see Appendix A for an analysis). Also note, for  $\kappa > 0$ ,  $\dot{\delta} < 0$  and so even when  $\mathring{H} \neq 0$ , we expect a solution where  $\delta$  approaches zero. If indeed  $\delta \rightarrow 0$ , then (22) implies

$$s \approx \delta e^{-\beta_1+1/2} + \mathcal{O}(\delta^3) \quad (91)$$

for all  $\mathring{H}$ ; i.e., as for  $\mathring{H} = 0$ ,  $\delta$  must go to zero with  $s$  along the line

$$s = \delta e^{-\beta_1+1/2}, \quad (92)$$

while from (67)  $\kappa$  must diverge as

$$\frac{c_2}{2}\kappa = \mathring{C} + \frac{c_1}{\delta} e^{\beta_1-1/2}. \quad (93)$$

Note, the sign of the righthand side of (68) is definite provided  $\mathring{C} > 0$  and  $\delta > 0$ .

Let us explore further the behavior for small  $\delta$ . To this end we use

$$\operatorname{erf}(\sqrt{y}) = \frac{2}{\sqrt{\pi}} \sum_{n=0}^{\infty} \frac{(-1)^n y^{n+1/2}}{n! (2n+1)},$$

for small  $y \in \mathbb{R}_+$ ,  $\sqrt{y} \operatorname{erf}(\sqrt{y}) \in C^\omega$ , and the identities are

$$\frac{d}{dx} \operatorname{erf}(x) = \frac{2}{\sqrt{\pi}} e^{-x^2} \quad \text{and} \quad \operatorname{erf}(x) = \frac{d}{dx} \left( x \operatorname{erf}(x) + \frac{e^{-x^2}}{\sqrt{\pi}} \right). \quad (94)$$

Upon multiplying (68) by  $\delta$  and defining  $u = \delta^2/2$ , it takes the form

$$\dot{u} = u^{\frac{1}{2}} g(u) - f(u) \quad (95)$$

where  $f, g \in C^\omega(\mathbb{R})$  are defined by

$$f(u) = e^{-2\mathring{H}u+2\beta_1-1} c_1 \left( \sqrt{2\pi\mathring{H}u} \operatorname{erf} \left( \sqrt{2\mathring{H}u} \right) + e^{-2\mathring{H}u} \right) \quad (96)$$

$$g(u) = -e^{-2\mathring{H}u+\beta_1-1/2} \sqrt{2} \mathring{C}, \quad (97)$$

and satisfy

$$f(0) = c_1 e^{2\beta_1-1} \quad \text{and} \quad g(0) = -\sqrt{2} \mathring{C} e^{\beta_1-1/2}. \quad (98)$$

Using (94) we see that the function  $f(u)$  is positive and monotonically decreasing, while the function  $g(u)$  has a sign determined by the sign of  $\mathring{C}$ , and is at least monotonic for small argument.

The functions  $f$  and  $g$  are depicted in Fig. 10.

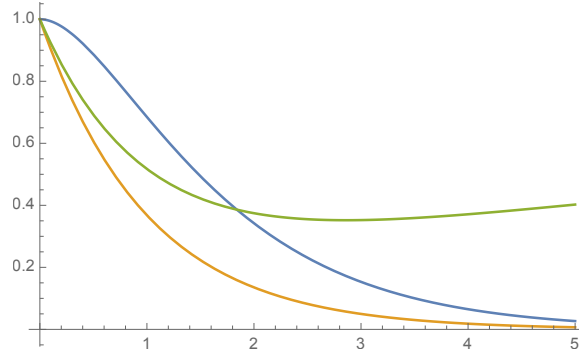


FIG. 10. Plots of  $\bar{f} = e^{-x}(\sqrt{\pi x} \operatorname{erf}(\sqrt{x}) + e^{-x})$  (blue),  $\bar{g} = 0.10 \times e^{-x}$  (orange), and  $\bar{f}/\bar{g} = \sqrt{\pi x} \operatorname{erf}(\sqrt{x}) + e^{-x}$  (green) vs.  $x = 2\mathring{H}u$ . Note,  $\sqrt{u_\infty} \sim \bar{f}(u_\infty)/\bar{g}(u_\infty)$  are the equilibria points corresponding to  $\kappa = 0$ .

Thus, near  $u = 0$  the MK system behaves as

$$\dot{u} = u^{\frac{1}{2}}g(0) - f(0) \quad (99)$$

Because  $u^{\frac{1}{2}}g(0) - f(0)$  is not Lipschitz on  $u \in [0, \epsilon]$  with  $\epsilon > 0$ , we do not have the usual ODE existence theorem to rely on (see e.g. [25]). If  $u(0) = \mathring{u} > 0$  is small, then  $\dot{u}(0) = \mathring{u}^{\frac{1}{2}}g(0) - f(0) < 0$ , because  $c_1 > 0$ , and  $u$  should decrease. However, the Lipschitz condition for uniqueness is a sufficient but not a necessary condition. Thus, further analysis is necessary, but indeed (99) does have a unique solution. To see this let  $u_1$  and  $u_2$  be two solutions that coincide at some time. A measure of their difference

$$D = \left( \sqrt{u_1(t)} - \sqrt{u_2(t)} \right)^2 \quad (100)$$

satisfies  $\dot{D} = 0$  for all time, so they must coincide.

From (99) we see there is a family of equilibrium points given by

$$\sqrt{u_0} = \frac{f(0)}{g(0)} = \frac{c_1 e^{\beta_1 - 1/2}}{\sqrt{2} \mathring{C}} \quad (101)$$

which only exists for  $\mathring{C} > 0$ . However, these are merely the  $\kappa = 0$  solutions mentioned above. In Appendix A it is seen that linearization about any of these equilibrium solutions

yields a spectrum with two zero eigenvalues and one unstable (positive) eigenvalue. This implies  $\kappa$  will grow so as to decrease the radius of curvature.

In any event, it is a simple matter to integrate (99), yielding

$$\frac{2}{g(0)} \left[ u^{\frac{1}{2}} + \frac{f(0)}{g(0)} \ln \left( 1 - u^{\frac{1}{2}} g(0)/f(0) \right) \right] = t + \text{const}, \quad (102)$$

which, upon expanding, gives for small  $u$

$$\delta \sim \sqrt{2f(0)(t_\infty - t)} = e^{\beta_1 - 1/2} \sqrt{2c_1(t_\infty - t)}. \quad (103)$$

the solution with Leray scaling consistent with (90) and (79).

## V. CONCLUSIONS

We have shown that the system put forth by Moffat and Kimura [1, 2] for the interaction of two tilted vortex rings has solutions with finite-time singularity. This was achieved by finding the noncanonical Hamiltonian structure of the equations, which naturally led to a geometrical depiction and explicit forms for the solutions by making use of the newly discovered Hamiltonian and Casimir invariants. Exact Leray divergence was demonstrated, within the inequalities proposed in [1, 2] for the model.

Several avenues for future work remain: in future publications we will consider the effect of viscous dissipation, further physical interpretation of the results, and various bounds and perturbation expansions. Of particular interest is to derive the Hamiltonian structure that we have obtained for the Moffat and Kimura model from that of Euler's equation. This will elucidate how the Hamiltonian and Casimir of the reduced model relate to those of the parent model. Insights about vortex lines and Casimirs described in [26], may be of particular help in this regard.

## ACKNOWLEDGMENT

PJM was supported by U.S. Dept. of Energy Contract # DE-FG05-80ET-53088 and a Forschungspreis from the Alexander von Humboldt Foundation. YK acknowledges support from JSPS KAKENHI grant #19H00641 and #16H06339.



## Appendix A: Non-Hamiltonian spectrum

Usually one studies the equilibrium points of a dynamical system in order to get a view into the nature of trajectories in phase space. Thus we study the only equilibrium point of (1), (2), and (3), viz.  $\kappa = 0$ , for any values of  $\delta$  and  $s$ , which corresponds to the vortex rings having infinite radii. Interestingly, although our system of equations (1), (2), and (3) is a Hamiltonian system, it has an associated singular Poisson tensor at this equilibrium point. As discussed in [21, 24], such systems may not have the usual Hamiltonian spectra when expanded about an equilibrium state, i.e., the symmetry of growing and decaying eigenvalues having the same magnitude.

The singularity occurs at  $\kappa = 0$  for any values of  $\delta$  and  $s$ . Such co-dimension one singularities may have the peculiar spectra. This kind of singularity follows because the Poisson tensor  $J$ , as given by  $\mathbf{V}$ , vanishes identically for  $\kappa = 0$ . This is seen because the components  $V_i$  for  $i = 1, 2, 3$  are all proportional to  $\kappa$ . At other points of phase space it has rank 2, while along this line rank zero.

The only equilibria of our system occur along the line  $\kappa = 0$ , while any values of  $\delta$  and  $s$  are allowed. Thus expanding as

$$s = s_0 + \tilde{s}, \quad \delta = \delta_0 + \tilde{\delta}, \quad \text{and} \quad \kappa = \tilde{\kappa} \quad (\text{A1})$$

we obtain a simple eigenvalue problem

$$\begin{bmatrix} \dot{\tilde{\delta}} \\ \dot{\tilde{s}} \\ \dot{\tilde{\kappa}} \end{bmatrix} = \begin{bmatrix} 0 & 0 & a \\ 0 & 0 & b \\ 0 & 0 & L \end{bmatrix} \begin{bmatrix} \tilde{\delta} \\ \tilde{s} \\ \tilde{\kappa} \end{bmatrix}, \quad (\text{A2})$$

where

$$a = -\frac{c_2 \delta_0}{2s_0}, \quad b = -c_2(\ln(s_0/\delta_0) + \beta_1), \quad \text{and} \quad L = \frac{c_1}{s_0^2},$$

with the matrix

$$\mathbb{M} := \begin{bmatrix} 0 & 0 & a \\ 0 & 0 & b \\ 0 & 0 & L \end{bmatrix}$$

giving rise to following characteristic polynomial by assuming temporal behavior of  $e^{\gamma t}$

$$\gamma^2(\gamma - c_1/s_0^2) = 0. \quad (\text{A3})$$

Thus the spectrum of  $M$  is  $\{0, 0, c_1/s_0^2\}$ .

In the right coordinates  $\mathbb{M}$  is the direct sum of commuting diagonal (semisimple) and nilpotent pieces. To this end we change coordinates by replacing  $\tilde{\delta}$  and  $\tilde{s}$ , while retaining  $\tilde{\kappa}$ , as follows;

$$\bar{\delta} = \tilde{\delta} - \frac{a}{L}\tilde{\kappa} \quad \text{and} \quad \bar{s} := \tilde{s} - \frac{b}{L}\tilde{\kappa}$$

in which case  $\mathbb{M}$  is replaced by

$$\bar{\mathbb{M}} := \begin{bmatrix} 0 & 0 & 0 \\ 0 & 0 & 0 \\ 0 & 0 & L \end{bmatrix}$$

and the linear dynamics is trivial. With  $\tilde{\kappa}$  exponentiating away at fixed initial  $\bar{\delta}$  and  $\bar{s}$ . From this we conclude that the rings will initially exponentially decrease their radii of curvature while  $\delta$  and  $s$  decrease.

## Appendix B: The Leray Hamiltonian

In light of Sec. [IV D](#), we observed that for small  $\delta$  the system exhibits Leray scaling. This behavior follows upon expanding [\(69\)](#) or by approximating [\(1\)](#), [\(2\)](#), and [\(3\)](#). Here we follow the second route, using in the vicinity of the singularity  $s \sim e^{1/2-\beta_1}\delta =: r\delta$ , to obtain the following set of equations that describe the dynamics near the singularity:

$$\dot{\delta} = -\frac{c_2}{2r}\kappa + \frac{\varepsilon}{2\delta} \tag{B1}$$

$$\dot{\kappa} = \frac{c_1}{r^2} \frac{\kappa}{\delta^2}. \tag{B2}$$

Upon setting  $\varepsilon = 0$  (future work considers its retention), we expect this reduced system of [\(B1\)](#) and [\(B2\)](#) to be Hamiltonian. Indeed, it conserves the quantity

$$\mathfrak{c} = \frac{c_2}{2}\kappa - \frac{c_1}{r\delta}, \tag{B3}$$

which upon using [\(42\)](#) and [\(54\)](#) can be shown to be the Casimir of [\(49\)](#) expanded to leading order, and [\(B1\)](#) and [\(B2\)](#) can be written in the noncanonical Hamiltonian form as

$$\begin{bmatrix} \dot{\delta} \\ \dot{\kappa} \end{bmatrix} = \begin{bmatrix} 0 & -\kappa/r \\ \kappa/r & 0 \end{bmatrix} \begin{bmatrix} \partial\mathfrak{c}/\partial\delta \\ \partial\mathfrak{c}/\partial\kappa \end{bmatrix} = \begin{bmatrix} 0 & -\kappa/r \\ \kappa/r & 0 \end{bmatrix} \begin{bmatrix} c_1/(r\delta^2) \\ c_2/2 \end{bmatrix}. \tag{B4}$$

Upon changing variables according to

$$q = r\delta \quad \text{and} \quad p = -\ln(\kappa) \quad (\text{B5})$$

the following canonical Hamiltonian form is obtained:

$$\dot{q} = \frac{\partial \mathfrak{c}}{\partial p} = -\frac{c_2}{2}e^{-p} \quad \text{and} \quad \dot{p} = -\frac{\partial \mathfrak{c}}{\partial q} = -\frac{c_1}{q^2} \quad (\text{B6})$$

where the Hamiltonian in canonical coordinates is

$$\mathfrak{c} = \frac{c_2}{2}e^{-p} - \frac{c_1}{q}. \quad (\text{B7})$$

Various canonical coordinate changes are possible, but given that there is a simple quadrature, they do not add insight. Clearly, upon setting  $\mathfrak{c}$  to a constant,  $\mathring{\mathfrak{c}}$ , and solving for  $p$ , as is usual for natural Hamiltonians of the form of (B7), we obtain the quadrature

$$\int \frac{dq}{\mathring{\mathfrak{c}}q + c_1} = - \int dt, \quad (\text{B8})$$

leading, yet again, to the Leray solution

$$q = r\delta \sim \sqrt{2c_1(t_\infty - t)}, \quad (\text{B9})$$

with  $\kappa$  following from  $\mathfrak{c} = \mathring{\mathfrak{c}}$ ,

$$\mathring{\mathfrak{c}} + \frac{c_1}{q} \sim \frac{c_1}{q} = \frac{c_2}{2}e^{-p} = \frac{c_2}{2}\kappa \quad \Rightarrow \quad \kappa \sim \sqrt{\frac{2c_1}{c_2^2(t_\infty - t)}}. \quad (\text{B10})$$

### Appendix C: Using $\kappa$ as a clock

There are various paths to quadrature. Here we present one where the system is transformed so that  $\kappa$  measures time. This is done by dividing (6) and (7) by (8), giving

$$\frac{d\delta}{d\bar{\kappa}} = -s\delta = -x\delta^2 \quad (\text{C1})$$

$$\frac{ds}{d\bar{\kappa}} = -s^2 \left[ \ln\left(\frac{s}{\delta}\right) + \beta_1 \right] = -s^2\Lambda \quad (\text{C2})$$

where  $\bar{\kappa} = c_2\kappa/c_1$ . Using (9) we can replace (C2) by

$$\frac{dx}{d\bar{\kappa}} = -\delta x(\Lambda - 1/2). \quad (\text{C3})$$

Next, because  $H$  is  $\kappa$  independent, we can use (21) in (C1) to obtain the quadrature

$$\frac{d\delta}{d\bar{\kappa}} = -\frac{e^{1/2-\beta_1}}{2} \delta^2 e^{\delta^2 \mathring{H}} \Rightarrow \int_{\delta}^{\delta} \frac{e^{-\delta'^2 \mathring{H}}}{\delta'^2} d\delta' = -\frac{e^{1/2-\beta_1}}{2} \int_{\bar{\kappa}}^{\bar{\kappa}} d\bar{\kappa}'. \quad (\text{C4})$$

With the substitution  $u = \delta^2 \mathring{H}$ , (C4) becomes

$$\int_{\mathring{H}\delta^2}^{\mathring{H}\delta^2} \frac{e^{-u'}}{u'^{3/2}} du' = -\frac{c_2}{c_1} \frac{e^{1/2-\beta_1}}{\sqrt{\mathring{H}}} (\kappa - \bar{\kappa}). \quad (\text{C5})$$

The lefthand side of (C5) can be written in terms of the incomplete gamma or error function defined by (40). Then, inverting (C5) for  $\delta(\kappa)$  and inserting into (C3) gives the following separable equation:

$$\frac{dx}{d\kappa} = -\frac{c_2}{c_1} x (\Lambda(x) - 1/2) \delta(\kappa), \quad (\text{C6})$$

the solution of which yields  $x(\kappa)$ , whence we obtain  $s = x\delta$  implying  $s(\kappa)$ . Finally, upon inserting  $s(\kappa)$  into (8), we can obtain  $\kappa(t)$ , and all quantities are known as functions of time.

- 
- [1] H. K. Moffatt and Y. Kimura. Towards a finite-time singularity of the Navier-Stokes equations Part 1. Derivation and analysis of dynamical system. *J. Fluid. Mech.*, 861:930–962, 2019.
  - [2] H. K. Moffatt and Y. Kimura. Towards a finite-time singularity of the Navier-Stokes equations Part 2. Vortex reconnection and singularity evasion. *J. Fluid. Mech.*, 870:R1, 2019.
  - [3] P. J. Morrison. Hamiltonian description of the ideal fluid. *Rev. Mod. Phys.*, 70:467–521, 1998.
  - [4] C. R. Doering. The 3D Navier-Stokes problem. *Annu. Rev. Fluid Mech.*, 41:109–128, 2009.
  - [5] J. T. Beale, T. Kato, and A. Majda. Remarks on the breakdown of smooth solutions for the 3D Euler equations. *Commun. Math. Phys.*, 94:61–66., 1984.
  - [6] S. Kida and M. Takaoka. Vortex reconnection. *Annu. Rev. Fluid Mech.*, 26:169–189, 1994.
  - [7] R. M. Kerr. Vortex collapse and turbulence. *Fluid Dyn. Res.*, 36:249–260, 1994.
  - [8] F. Hussain and K. Duraisamy. Mechanics of viscous vortex reconnection. *Phys. Fluids*, 23:021701, 2011.
  - [9] G. P. Bewley, K. P. M. S. Paoletti, Sreenivasan, and D. P. Lathrop. Characterization of reconnecting vortices in superfluid helium. *Proc. Nat. Acad. Sci.*, 105:13707–13710, 2008.
  - [10] S. Zuccher, M. Caldari, A. W. Baggaley, and C. F. Barenghi. Quantum vortex reconnections. *Phys. Fluids*, 24, 2012.

- [11] A. Villois, D. Proment, and G. Krstulovic. Universal and non-universal aspects of vortex reconnections in superfluids. *Phys. Rev. F*, 2:125108, 2017.
- [12] E. D. Siggia and A. Pumir. Incipient singularities in the Navier-Stokes equations. *Phys. Rev. Lett*, 554:1749–1752, 1985.
- [13] R. B. Pelz, Y. Gulak Y, J. M. Greene, and O. N. Boratav. On the finite-time singularity problem in hydrodynamics. In A. Gyr, W. Kinzelbach, and A. Tsinober, editors, *Fundamental Problematic Issues in Turbulence*, Trends in Mathematics, pages 33–40, Basel, 1999. Birkhaeuser.
- [14] M. P. Brenner, S. Hormoz, and A. Pumir. Potential singularity mechanism for the Euler equations. *Phys. Rev. F*, 1:084503, 2016.
- [15] Y. Kimura and H. K. Moffatt. A tent model of vortex reconnection under Biot-Savart evolution. *J. Fluid Mech.*, 834:R1, 2018.
- [16] R. M. Kerr. Enstrophy and circulation scaling for Navier-Stokes reconnection. *J. Fluid Mech.*, 839:R2, 2018.
- [17] P. J. Morrison and J. M. Greene. Noncanonical Hamiltonian density formulation of hydrodynamics and ideal magnetohydrodynamics. *Phys. Rev. Lett.*, 45:790–793, 1980.
- [18] E. C. G. Sudarshan and N. Makunda. *Classical Dynamics: a modern perspective*. John Wiley & Sons, New York, 1974.
- [19] P. J. Morrison, T. Andreussi, and F. Pegoraro. Lagrangian and Dirac constraints for the ideal incompressible fluid and magnetohydrodynamics *J. Plasma Phys.*, 86:835860301, 2020.
- [20] A. Weinstein. The local structure of Poisson manifolds. *J. Diff. Geom.*, 18:523–557, 1983. Erratum 22:255, 1985.
- [21] Z. Yoshida and P. J. Morrison. Deformation of Lie-Poisson algebras and chirality. *J. Math. Phys.*, 61:082901, 2020.
- [22] Milton Abramowitz and Irene A. Stegun. *Handbook of Mathematical Functions with Formulas, Graphs, and Mathematical Tables*. Dover, New York City, ninth dover printing, tenth gpo printing edition, 1964.
- [23] S. P. Meacham, P. J. Morrison, and G. R. Flierl. Hamiltonian moment reduction for describing vortices in shear. *Phys. Fluids*, 9:2310–2328, 1997.
- [24] Z. Yoshida, T. Tokieda, and P. J. Morrison. Rattleback: A model of how geometric singularity induces dynamic chirality. *Phys. Lett. A*, 381:00, 2017.

- [25] E. A. Coddington and N. Levinson. *Theory of Ordinary Differential Equations*. McGraw-Hill, New York, 1955.
- [26] E. A. Kuznetsov and V. P. Ruban. Hamiltonian dynamics of vortex lines in hydrodynamic-type systems *JETP Letters*, 67:1076–1081, 1998.